

Theory of Spin Relaxation in Two-Electron Lateral Coupled Quantum Dots

Martin Raith,¹ Peter Stano,² Fabio Baruffa,^{1,3} and Jaroslav Fabian¹

¹*Institute for Theoretical Physics, University of Regensburg, D-93040 Regensburg, Germany*

²*Institute of Physics, Slovak Academy of Sciences, 845 11 Bratislava, Slovakia*

³*German Research School for Simulation Sciences, Forschungszentrum Juelich, D-52425 Germany*

(Received 29 November 2011; published 12 June 2012)

A global quantitative picture of the phonon-induced two-electron spin relaxation in GaAs double quantum dots is presented using highly accurate numerics. Wide regimes of interdot coupling, magnetic field magnitude and orientation, and detuning are explored in the presence of a nuclear bath. Most important, the giant magnetic anisotropy of the singlet-triplet relaxation can be controlled by detuning switching the principal anisotropy axes: a protected state becomes unprotected upon detuning and vice versa. It is also established that nuclear spins can dominate spin relaxation for unpolarized triplets even at high magnetic fields, contrary to common belief.

DOI: [10.1103/PhysRevLett.108.246602](https://doi.org/10.1103/PhysRevLett.108.246602)

PACS numbers: 72.25.Rb, 03.67.Lx, 71.70.Ej, 73.21.La

Electron spins in quantum dots [1] are among perspective candidates for a controllable quantum coherent system in spintronics [2,3]. Spin qubits in GaAs quantum dots, the current state of the art [4,5], are coupled to two main environment baths: nuclear spins and phonons [6]. The nuclei dominate decoherence, which is on microsecond time scales. But only phonons are an efficient energy sink for the relaxation of the energy-resolved spin states, leading to spin lifetimes as long as seconds [7].

The extraordinary low relaxation is boosted by orders of magnitude at spectral crossings, unless special conditions—such geometries we call easy passages—are met [8,9]. Spectral crossings seem inevitable in the manipulation based on the Pauli spin blockade [1,10], the current choice in spin qubit experiments [11]. On the other hand, a fast spin relaxation channel may be desired, e.g., in the dynamical nuclear polarization [12–14].

The single-electron spin relaxation is well understood [15,16]: it proceeds through acoustic phonons, in proportion to their density of states, which increases with the transferred energy. The matrix element of the phonon electric field between spin opposite states is nonzero due to spin-orbit coupling or nuclear spins. At anticrossings, the matrix element is enhanced by orders of magnitude, even though the anticrossing gap is minute ($\sim \mu\text{eV}$). The relaxation rate can be either enhanced or suppressed, depending on whether the energy or the matrix element effects dominate.

The two electron relaxation rates were measured in single [17–19] and in double [20–22] dots. Theoretical works so far mostly focused on single dots [23,24], or vertical double dots [25,26], in which the symmetry of the confinement potential lowers the numerical demands. A slightly deformed dot was considered in Refs. [27,28], and a lateral coupled double dot in silicon in Ref. [29]. What is key for spin-qubit manipulation and most relevant for ongoing experiments, is the case of weakly coupled and

biased coupled dots. In addition, the relative roles of the spin-orbit and hyperfine interactions in the spin relaxation in GaAs quantum dots have not yet been established.

The analysis of the two-electron double dot relaxation is challenging because many parameters need to be considered simultaneously: the magnitude and orientation of the magnetic field, the orientation of the dot with respect to the crystallographic axes, the strength of the interdot coupling (parametrized by either tunneling or exchange energy) and the bias applied across the double dot (detuning). Here we cover all these parameters, including the nuclear bath, providing specific relevant predictions for experimental setups [30]. Perhaps the most striking results are the existence of islands of inhibited spin relaxation in the magnetic field and detuning maps, and the switch of the two principal C_{2v} axes along which the relaxation shows a minimum or maximum, as detuning is turned on. While singlets and polarized triplets relax by spin-orbit coupling, the spin-unpolarized triplet relaxation is dominated by nuclear spins over a wide parameter range (the spin-orbit induced anisotropy is wiped out), contrary to common belief. The predicted giant spin relaxation anisotropy is a unique and experimentally testable signature of spin-orbit spin relaxation, which can also be useful for spin nano-devices, as we argue in this Letter.

Model.—We consider a laterally coupled, top-gated GaAs double quantum dot patterned in the plane perpendicular to $\hat{z} = [001]$. In the two-dimensional and envelope function approximation, the Hamiltonian reads

$$H = \sum_{i=1,2} (T_i + V_i + H_{Z,i} + H_{\text{so},i} + H_{\text{nuc},i}) + H_C, \quad (1)$$

where i labels electrons. The single-electron terms are

$$T = \mathbf{P}^2/2m = (-i\hbar\nabla + e\mathbf{A})^2/2m, \quad (2)$$

$$V = \frac{1}{2}m\omega_0^2 \min\{(\mathbf{r} - \mathbf{d})^2, (\mathbf{r} + \mathbf{d})^2\} + e\mathbf{E} \cdot \mathbf{r}, \quad (3)$$

$$H_Z = (g/2)\mu_B \boldsymbol{\sigma} \cdot \mathbf{B}, \quad (4)$$

$$H_{\text{so}} = H_{\text{BR}} + H_{\text{D}} + H_{\text{D3}}, \quad (5)$$

the kinetic energy, the biquadratic confinement potential, the Zeeman term, and the spin-orbit couplings, respectively. The position and momentum vectors are two-dimensional, where $\hat{\mathbf{x}} = [100]$ and $\hat{\mathbf{y}} = [010]$. The proton charge is e and the effective electron mass is m . The confinement energy, $E_0 = \hbar\omega_0$, and the confinement length, $l_0 = (\hbar/m\omega_0)^{1/2}$, define the characteristic scales. The potential is minimal at $\pm \mathbf{d}$, and we call $2d/l_0$ the interdot distance. The electric field \mathbf{E} is applied along the dot main axis \mathbf{d} . Turning on \mathbf{E} shifts the potential minima relative to each other by the detuning energy $\epsilon = 2eEd$. The magnetic field is $\mathbf{B} = (B_x, B_y, B_z)$. We use the symmetric gauge, $\mathbf{A} = B_z(-y, x)/2$, and $\boldsymbol{\sigma} = (\sigma_x, \sigma_y, \sigma_z)$ are the Pauli matrices. The Landé factor is g , and the Bohr magneton is μ_B . The Bychkov-Rashba, and the linear and cubic Dresselhaus Hamiltonian read

$$H_{\text{BR}} = (\hbar/2ml_{\text{BR}})(\sigma_x P_y - \sigma_y P_x), \quad (6)$$

$$H_{\text{D}} = (\hbar/2ml_{\text{D}})(-\sigma_x P_x + \sigma_y P_y), \quad (7)$$

$$H_{\text{D3}} = (\gamma_c/2\hbar^3)(\sigma_x P_x P_y^2 - \sigma_y P_y P_x^2) + \text{H.c.}, \quad (8)$$

parametrized by the spin-orbit lengths l_{BR} and l_{D} , and a bulk parameter γ_c . Nuclei, labeled by n , couple through

$$H_{\text{nuc}} = \beta \sum_n \mathbf{I}_n \cdot \boldsymbol{\sigma} \delta(\mathbf{r} - \mathbf{R}_n), \quad (9)$$

where β is a constant, and \mathbf{I}_n is the spin of a nucleus at the position \mathbf{R}_n . The Coulomb interaction is $H_C = e^2/4\pi\epsilon|\mathbf{r}_1 - \mathbf{r}_2|$, with the material dielectric constant ϵ . The Hamiltonian, Eq. (1), and its energy spectrum are discussed in Refs. [31,32], including our numerical method (configuration interaction) for its diagonalization. Here we extend it by including nuclear spins, which we treat by averaging over unpolarized random ensemble. See Supplemental Material [33] for further details.

The relaxation is mediated by acoustic phonons

$$H_{\text{ep}} = i \sum_{\mathbf{Q}, \lambda} \sqrt{\frac{\hbar Q}{2\rho V c_\lambda}} V_{\mathbf{Q}, \lambda} [b_{\mathbf{Q}, \lambda}^\dagger e^{i\mathbf{Q} \cdot \mathbf{R}} - b_{\mathbf{Q}, \lambda} e^{-i\mathbf{Q} \cdot \mathbf{R}}], \quad (10)$$

with deformation, $V_{\mathbf{Q}, l}^{\text{df}} = \sigma_e$, and piezoelectric potentials, $V_{\mathbf{Q}, \lambda}^{\text{pz}} = -2ie h_{14}(q_x q_y \hat{e}_{\mathbf{Q}, z}^\lambda + q_z q_x \hat{e}_{\mathbf{Q}, y}^\lambda + q_y q_z \hat{e}_{\mathbf{Q}, x}^\lambda)/Q^3$. The phonon wave vector is \mathbf{Q} , and the electron position vector is $\mathbf{R} = (\mathbf{r}, z)$. The polarizations are given by λ , the polarization unit vector reads $\hat{\mathbf{e}}$, and the phonon annihilation (creation) operator is denoted by b (b^\dagger). The mass density, the volume of the crystal, and the sound velocities are given by ρ , V , and c_λ , respectively. The phonon potentials are parametrized by σ_e , and h_{14} .

We define the relaxation rate as the sum of the individual transition rates to all lower-lying states for both

piezoelectric and deformation potentials. Each rate (from $|i\rangle$ to $|j\rangle$) is evaluated using the Fermi golden rule in the zero-temperature limit,

$$\Gamma_{ij} = \frac{\pi}{\hbar \rho V} \sum_{\mathbf{Q}, \lambda} \frac{Q}{c_\lambda} |V_{\mathbf{Q}, \lambda}|^2 |M_{ij}|^2 \delta(\omega_{ij} - \omega_{\mathbf{Q}}), \quad (11)$$

where $M_{ij} = \langle i | e^{i\mathbf{Q} \cdot \mathbf{R}} | j \rangle$ is the matrix element of the states with energy difference $\hbar\omega_{ij}$. Here we are interested in the rates of the singlet (S) and the three triplets (T_+ , T_0 , T_-) at the bottom of the energy spectrum.

In numerics, we use GaAs parameters: $m = 0.067m_e$, with m_e the free electron mass, $g = -0.44$, $c_l = 5290$ m/s, $c_t = 2480$ m/s, $\rho = 5300$ kg/m³, $\sigma_e = 7$ eV, $eh_{14} = 1.4 \times 10^9$ eV/m, $\epsilon = 12.9\epsilon_0$, $\gamma_c = 27.5$ eVÅ³, $\beta = 2$ μ eVnm³, $l = 3/2$. We choose typical lateral dot values, $l_{\text{BR}} = 2.42$ μ m, $l_{\text{D}} = 0.63$ μ m, $\mathbf{d} || [110]$ and the confinement energy $E_0 = 1.0$ meV, corresponding to $l_0 = 34$ nm.

Results.—We start with an unbiased double dot. We plot its spectrum in Fig. 1(a) as a function of the interdot coupling, which translates into an exponentially sensitive S - T_0 exchange splitting J . Electrical control over J , necessary e.g. to induce the $\sqrt{\text{SWAP}}$ gate [1], allows for a fast switching between the strong and weak coupling regime, corresponding to the exchange splitting being larger and smaller than the Zeeman energy, respectively. During this switching, the ground state changes at an S - T_+ anticrossing.

We cover the freedom of the interdot coupling in Fig. 2. Panel a) shows the relaxation of the first excited state [S or T_+ , see Fig. 1(a)]. First to note is the strong relaxation suppression at the S - T_+ anticrossing as the transferred energy becomes very small. Remarkably, the anticrossing does not influence the rate of T_0 , plotted at panel b), at all (the peak close to $d = 0$ is due to an anticrossing with a higher excited state). Even though the dominant channel, $T_0 \rightarrow T_+$, is strongly suppressed here, its reduction is exactly compensated by the elsewhere negligible $T_0 \rightarrow S$

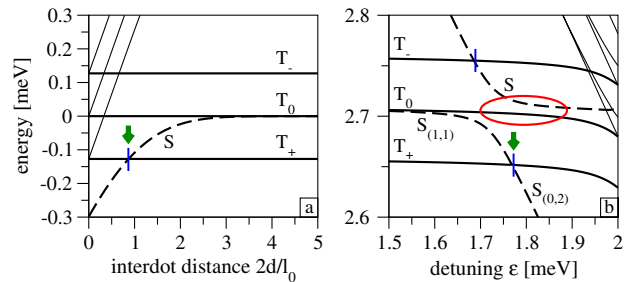


FIG. 1 (color online). Calculated energies of the lowest states for (a) variable interdot coupling (at $B = 5$ T) and (b) detuning (at $B = 2$ T). Singlet states are given by dashed lines, triplets by solid lines. The blue strokes mark singlet-triplet anticrossings. In (a), the energy of T_0 is subtracted, and in (b), the quadratic trend in E is subtracted. The green arrows denote points of exact compensation, and the red oval in (b) shows where nuclear spins dominate the T_0 relaxation.

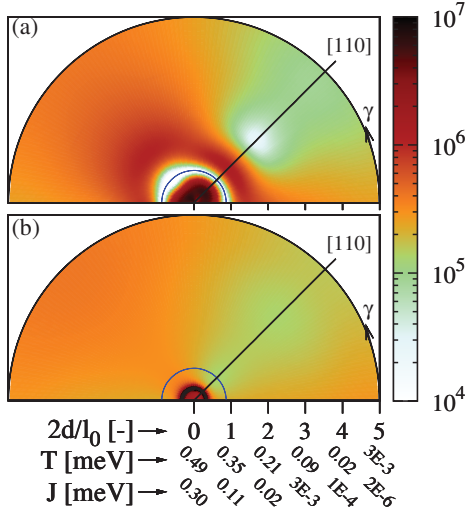


FIG. 2 (color). Calculated relaxation rates of (a) the first excited state [S or T_+ , see Fig. 1(a)] and (b) the triplet T_0 as a function of the in-plane magnetic field orientation $\gamma = \arccos(B_x/B)$ (angle) and the interdot distance $2d/l_0$ (radius of the polar plot), for a double dot at $B = 5$ T. The x and y axes correspond to crystallographic axes $[100]$ and $[010]$, respectively. The dot orientation $\mathbf{d} \parallel [110]$ is marked by a line. The blue half circles indicate the S - T_+ anticrossing, also marked on Fig. 1(a). The x axis is converted to the tunneling energy T and the exchange J , in addition to $2d/l_0$. The rate is given in inverse seconds by the color scale. The system obeys C_{2v} symmetry, so point reflection would complete the graphs.

channel. The exact compensation arises for the relaxation into a quasi-degenerate subspace (we denote such cases on Fig. 1 by green arrows) if

$$\Delta E \ll \min\{E, \hbar c_\lambda/l_0\}. \quad (12)$$

Here E is the transition energy and ΔE is the energy width of subspace (the anticrossing gap). Equation (12) states that the energy width ΔE is too small to be resolved by either phonons with energy E or electron wave function scale l_0 [33]. The relaxation then proceeds into the subspace rather than into its constituent states, so that any mixing of the states within the subspace is irrelevant.

Further to note on Fig. 2 is the anisotropy of relaxation, which reflects the anisotropy of the spin-orbit fields. In the weak coupling regime, the relaxation rates are minimal if the magnetic field orientation is parallel to the dot main axis, which results in an isle of strongly prolonged spin lifetimes. Note that this is in contrast to the biased dot (see below), and to the single-electron case, where the minimal in-plane magnetic field direction, the easy passage, of a $\mathbf{d} \parallel [110]$ double dot is perpendicular to \mathbf{d} [9,34]. The switch can be understood from the effective, spin-orbit induced, magnetic field [9] if written using the coordinates along the dot axes $x_d, y_d = (x \pm y)/\sqrt{2}$,

$$\mathbf{B}_{\text{so}} = \mathbf{B} \times \{x_d(l_{\text{BR}}^{-1} - l_{\text{D}}^{-1})[1\bar{1}0] + y_d(l_{\text{BR}}^{-1} + l_{\text{D}}^{-1}) \times [110]\}/\sqrt{2}. \quad (13)$$

At the anticrossing, the mixing due to x_d is by far dominant, so the minimum appears with \mathbf{B} along $[1\bar{1}0]$. This x_d dominance will be the case for a biased dot, too. On the other hand, in a single dot x_d and y_d induce comparable mixing, and \mathbf{B}_{so} becomes minimal if the larger term (the one with y_d) is eliminated. Weakly coupled unbiased dot is in this respect similar to a single dot as the two-electron transitions can be understood as flips of a particular electron located in a single dot. Since the direction for the rate minimum switches upon changing d , the system does not show an easy passage, that is a low relaxation rate from weak to strong coupling regime.

We plot the magnetic field dependence for a weakly coupled unbiased double dot in Fig. 3 and observe similar behavior as in Fig. 2. The relaxation rate is minimal if $\mathbf{B} \parallel \mathbf{d}$ throughout the shown parametric region. This is because the anticrossing and the related directional switch happens here at so small magnetic field that it is not visible at the figure resolution. For completeness, we note that the T_- relaxation behavior is very similar to the one for T_0 on both Figs. 2 and 3, and we do not show it.

We now consider a biased double dot. Its spectrum is shown in Fig. 1(b) as a function of the detuning. The ground state singlet is in the (1,1) configuration (one electron in each dot) for low, and in the (0,2) configuration (both electrons in one dot) for large detunings. The crossover, a broad singlet-singlet anticrossing, is a key handle in spin measurement and manipulation [11]. The low to large detuning crossover involves S - T_\pm anticrossing, exploited for nuclear-spin pumping [12,35].

We show the detuning and magnetic field influence on the relaxation in Fig. 4. At the singlet-triplet anticrossings, we observe that first, the relaxation rate of the first

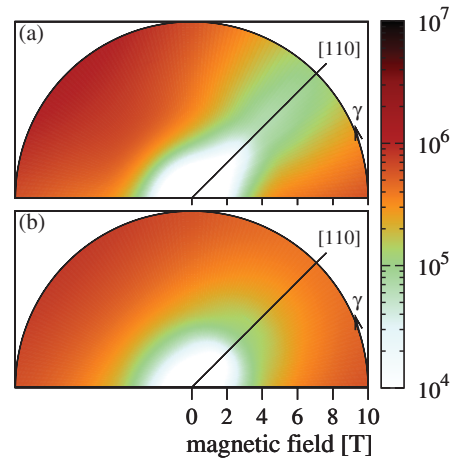


FIG. 3 (color). Calculated relaxation rates of (a) the first excited state and (b) the triplet T_0 as a function of the in-plane magnetic field orientation γ (angle) and the magnetic field magnitude (radius of the polar plot) for a double dot with $T = 0.1$ meV. The layout with respect to the crystallographic axes is the same as in Fig. 2. The rate is given in inverse seconds by the color scale.

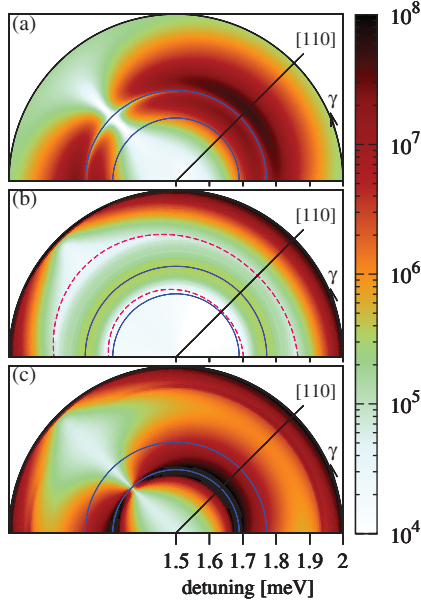


FIG. 4 (color). Calculated relaxation rates of (a) the first excited state, (b) T_0 , and (c) T_- as a function of the in-plane magnetic field orientation γ (angle) and detuning energy (radius of the polar plot), for a double dot with $2d/l_0 = 4.35$ ($T = 10 \mu\text{eV}$), chosen along Ref. [11], and $B = 2$ T. The layout with respect to the crystallographic axes is the same as in Fig. 2. The rate is given in inverse seconds by the color scale. The blue lines indicate the singlet-triplet anticrossings, which are in line with the marks in Fig. 1(b). The dashed red lines in panel (b) confine the area where hyperfine coupling dominates.

excited state dips at the $S-T_+$ anticrossing (though the dip is very narrow and hard to see at the figure resolution), and second, the T_- rate strongly peaks at the $S-T_-$ anticrossing. This is a demonstration of the dominant effect of the anticrossing on the transition energy, and matrix element, respectively. Third, there are no other manifestations of the $S-T_{\pm}$ anticrossings, a fact due to the exact compensation already mentioned before. The anisotropy features of this geometry are striking. In the given range of detuning energies, states except T_0 exhibit a very distinctive easy passage for a magnetic field along $[1\bar{1}0]$, where the relaxation is up to to three orders of magnitude smaller than with \mathbf{B} along $[110]$. Though the directional switch occurs—rates become minimal for a magnetic field along $[110]$, it is again out of the figure scope (very small and very large detunings). The rates increase at detunings ≥ 2 meV, because of spectral crossings with excited triplets, Fig. 1(b), regime normally avoided in experiments. Double dots, with their spectral idiosyncrasies, are a unique system to observe a giant amplification of the spin-orbit anisotropies by a physical observable with bias control.

In large parts of the parametric space, the relaxation of T_0 is dominated by nuclear spins, thus being isotropic. This is surprising, since the effective (Overhauser) nuclear magnetic field B_{nuc} is of the order of mT, much smaller than the

spin-orbit field in Eq. (13), $B_{\text{so}} \sim (l_0/l_{\text{so}})B \approx 30$ mT at $B = 1$ T for our parameters. One therefore expects the nuclei to lead to much slower relaxation than the spin-orbit coupling. This was indeed the case for the unbiased dots and Figs. 2 and 3. How then can nuclei dominate here? Looking on Fig. 1(b), this happens when states T_0 and $S(1, 1)$ are nearby in energy. Here, the otherwise negligible hyperfine effects take over, because the spin-orbit induced mixing of these two states is forbidden [27]. Estimating the wave function admixture in the lowest order, the nuclei dominate if

$$B_{\text{so}}/|E_{T_0} - E_k| \lesssim B_{\text{nuc}}/|E_{T_0} - E_S|, \quad (14)$$

with k being the closest state to which T_0 is coupled by the spin-orbit interaction. The above condition generalizes in an obvious way for other states than T_0 and there are additional cases of nuclear dominance in our system. However, they happen on parameter regions too small to be visible on the resolution of Fig. 4, so we discuss them only in the Supplemental Material [33].

Our predictions are experimentally observable. Until now the spin-orbit origin, and especially its induced directional anisotropy of the spin relaxation in weakly coupled two-electron dots, has not yet been experimentally established. With employing vector magnets, it should now be possible to overcome earlier experimental challenges and change the magnetic field orientation while keeping the sample fixed and detect the anisotropy [36]. The spin-orbit or nuclear-induced relaxation can be masked by cotunneling and smeared by a finite temperature. The former is reduced in the charge sensing readout setups [37], in which the coupling to the leads can be made small. The latter effect is small for experimentally relevant subkelvin temperatures, such that the directional anisotropies are well preserved.

Our results demonstrate control over the spin-orbit induced anticrossing gaps (easy passages appear if the gaps are closed) by sample and magnetic field geometry. It offers electrical tunability of spin relaxation, by changing the double dot orientation (in the Supplemental Material [33], we suggest a spin current measurement device exploiting easy passage). In addition, such control may be especially useful when dealing with hyperfine spins. Indeed, in the polarization scheme considered in Ref. [14], the nuclear spin polarization is proportional to nonhyperfine assisted spin relaxation (see Eq. (7) therein) and so would benefit from a setup with maximized spin-orbit induced relaxation rates (out of the easy passage). On the other hand, the adiabatic pumping scheme demonstrated in Ref. [35] relies on the $S - T_+$ anticrossing being solely due to the nuclear spins (and not the spin-orbit coupling), suggesting improved efficiency in an easy passage configuration. We propose a similar nonadiabatic nuclear pumping scheme based on the easy passage in the Supplemental Material [33]. All these examples

illustrate the potential benefits that intentional control of spin relaxation, based on our results, may offer.

This work was supported by DFG under Grants No. SPP 1285 and No. SFB 689. P. S. acknowledges support by meta-QUTE ITMS NFP 26240120022, CE SAS QUTE, EU Project Q-essence, APVV-0646-10, and SCIEEX.

-
- [1] D. Loss and D.P. DiVincenzo, *Phys. Rev. A* **57**, 120 (1998).
- [2] I. Žutić, J. Fabian, and S. Das Sarma, *Rev. Mod. Phys.* **76**, 323 (2004).
- [3] J. Fabian, A. Matos-Abiague, C. Ertler, P. Stano, and I. Žutić, *Acta Phys. Slovaca* **57**, 565 (2007).
- [4] R. Hanson, L.P. Kouwenhoven, J.R. Petta, S. Tarucha, and L.M.K. Vandersypen, *Rev. Mod. Phys.* **79**, 1217 (2007).
- [5] R. Brunner, Y.-S. Shin, T. Obata, M. Pioro-Ladrière, T. Kubo, K. Yoshida, T. Taniyama, Y. Tokura, and S. Tarucha, *Phys. Rev. Lett.* **107**, 146801 (2011).
- [6] A.V. Khaetskii and Y.V. Nazarov, *Phys. Rev. B* **64**, 125316 (2001).
- [7] S. Amasha, K. MacLean, I.P. Radu, D.M. Zumbühl, M.A. Kastner, M.P. Hanson, and A.C. Gossard, *Phys. Rev. Lett.* **100**, 046803 (2008).
- [8] V.N. Golovach, A. Khaetskii, and D. Loss, *Phys. Rev. Lett.* **93**, 016601 (2004).
- [9] P. Stano and J. Fabian, *Phys. Rev. Lett.* **96**, 186602 (2006).
- [10] X. Hu and S. Das Sarma, *Phys. Rev. A* **61**, 062301 (2000).
- [11] J.M. Taylor, J.R. Petta, A.C. Johnson, A. Yacoby, C.M. Marcus, and M.D. Lukin, *Phys. Rev. B* **76**, 035315 (2007).
- [12] A. Pfund, I. Shorubalko, K. Ensslin, and R. Leturcq, *Phys. Rev. Lett.* **99**, 036801 (2007).
- [13] M.S. Rudner and L.S. Levitov, *Phys. Rev. Lett.* **99**, 036602 (2007).
- [14] M.S. Rudner and L.S. Levitov, *Phys. Rev. Lett.* **99**, 246602 (2007).
- [15] J.M. Elzerman, R. Hanson, L.H. Willems van Beveren, B. Witkamp, L.M.K. Vandersypen, and L.P. Kouwenhoven, *Nature* **430**, 431 (2004).
- [16] P. Stano and J. Fabian, *Phys. Rev. B* **74**, 045320 (2006).
- [17] T. Fujisawa, D.G. Austing, Y. Tokura, Y. Hirayama, and S. Tarucha, *Nature* **419**, 278 (2002).
- [18] S. Sasaki, T. Fujisawa, T. Hayashi, and Y. Hirayama, *Phys. Rev. Lett.* **95**, 056803 (2005).
- [19] T. Meunier, I.T. Vink, L.H. Willems van Beveren, K.-J. Tielrooij, R. Hanson, F.H.L. Koppens, H.P. Tranitz, W. Wegscheider, L.P. Kouwenhoven, and L.M.K. Vandersypen, *Phys. Rev. Lett.* **98**, 126601 (2007).
- [20] J.R. Petta, A.C. Johnson, A. Yacoby, C.M. Marcus, M.P. Hanson, and A.C. Gossard, *Phys. Rev. B* **72**, 161301 (2005).
- [21] F.H.L. Koppens, J.A. Folk, J.M. Elzerman, R. Hanson, L.H.W. van Beveren, I.T. Vink, H.P. Tranitz, W. Wegscheider, L.P. Kouwenhoven, and L.M.K. Vandersypen, *Science* **309**, 1346 (2005).
- [22] A.C. Johnson, J.R. Petta, J.M. Taylor, A. Yacobi, M.D. Lukin, C.M. Marcus, M.P. Hanson, and A.C. Gossard, *Nature* **435**, 925 (2005).
- [23] J.I. Climente, A. Bertoni, G. Goldoni, M. Rontani, and E. Molinari, *Phys. Rev. B* **75**, 081303(R) (2007).
- [24] V.N. Golovach, A. Khaetskii, and D. Loss, *Phys. Rev. B* **77**, 045328 (2008).
- [25] D. Chaney and P.A. Maksym, *Phys. Rev. B* **75**, 035323 (2007).
- [26] K. Shen and M.W. Wu, *Phys. Rev. B* **76**, 235313 (2007).
- [27] M. Florescu and P. Hawrylak, *Phys. Rev. B* **73**, 045304 (2006).
- [28] O. Olencki and T.V. Shahbazyan, *Phys. Rev. B* **75**, 041306(R) (2007).
- [29] L. Wang and M.W. Wu, *J. Appl. Phys.* **110**, 043716 (2011).
- [30] We present the results for the state-of-the art GaAs quantum dots. We have also calculated the rates for silicon (unpublished), where the rates are orders of magnitude smaller but qualitatively the results are similar. Differences may arise for isotopically purified silicon dots, where nuclei effects are reduced.
- [31] F. Baruffa, P. Stano, and J. Fabian, *Phys. Rev. Lett.* **104**, 126401 (2010).
- [32] F. Baruffa, P. Stano, and J. Fabian, *Phys. Rev. B* **82**, 045311 (2010).
- [33] See Supplemental Material at <http://link.aps.org/supplemental/10.1103/PhysRevLett.108.246602> for details on the numerical method, a comparative comparison of hyperfine and spin-orbit induced relaxation, and examples of easy passage exploitations.
- [34] M. Raith, P. Stano, and J. Fabian, *Phys. Rev. B* **83**, 195318 (2011).
- [35] D.J. Reilly, J.M. Taylor, J.R. Petta, C.M. Marcus, M.P. Hanson, and A.C. Gossard, *Science* **321**, 817 (2008).
- [36] S. Amasha (private communication).
- [37] C. Barthel, D.J. Reilly, C.M. Marcus, M.P. Hanson, and A.C. Gossard, *Phys. Rev. Lett.* **103**, 160503 (2009).